Comparative analysis of TIG welding distortions between Austenitic and Duplex Stainless Steels by FEM

J.J. del Coz Díaz, P. Menéndez Rodríguez, P.J.García Nieto, D. Castro-Fresno

To cite this version:

J.J. del Coz Díaz, P. Menéndez Rodríguez, P.J.García Nieto, D. Castro-Fresno. Comparative analysis of TIG welding distortions between Austenitic and Duplex Stainless Steels by FEM. Applied Thermal Engineering, 2010, 30 (16), pp.2448. ⟨10.1016/j.applthermaleng.2010.06.016⟩. ⟨hal-00675405⟩

HAL Id: hal-00675405

https://hal.science/hal-00675405v1

Submitted on 1 Mar 2012

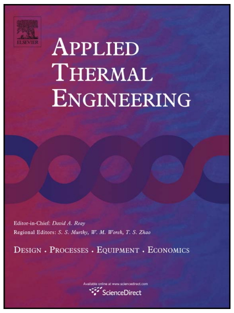

Title: Comparative analysis of TIG welding distortions between Austenitic and Duplex Stainless Steels by FEM

Authors: J.J. del Coz Díaz, P. Menéndez Rodríguez, P.J.García Nieto, D. Castro-Fresno

PII: S1359-4311(10)00263-2
DOI: 10.1016/j.applthermaleng.2010.06.016
Reference: ATE 3147

To appear in: *Applied Thermal Engineering*

Received Date: 1 February 2010
Revised Date: 24 May 2010
Accepted Date: 21 June 2010

Please cite this article as: J.J. del Coz Díaz, M. Rodríguez, G. Nieto, D. Castro-Fresno. Comparative analysis of TIG welding distortions between Austenitic and Duplex Stainless Steels by FEM, Applied Thermal Engineering (2010), doi: 10.1016/j.applthermaleng.2010.06.016

Comparative analysis of TIG welding distortions between Austenitic and Duplex Stainless Steels by FEM

J. J. del Coz Díaz[a], P. Menéndez Rodríguez[a], P. J. García Nieto[b], and D. Castro-Fresno[c]

[a]Department of Construction. University of Oviedo, 33204 Gijón, Spain
+34-985182042 – juanjo@constru.uniovi.es.
[b]Department of Mathematics. University of Oviedo, 33007 Oviedo, Spain
[c]Department of Construction.University of Cantabria. 39005 Santander, Spain

Abstract

In this study, thermal stress analyses were performed in the tungsten inert gas (TIG) welding process of two different stainless steel specimens in order to compare their distortion mode and magnitude. The growing presence of non-conventional stainless steel species like duplex family generates uncertainty about how their material properties could be affected under the welding process. To develop suitable welding numerical models, authors must consider the welding process parameters, geometrical constraints, material nonlinearities and all physical phenomena involved in welding, both thermal and structural. In this sense, four different premises are taken into account. Firstly, all finite elements corresponding to the deposition welding are deactivated and, next, they are reactivated according to the torch's movement to simulate mass addition from the filler metal into the weld pool. Secondly, the movement of the TIG torch was modelled in a discontinuous way assuming a constant welding speed. Thirdly, the arc heat input was applied to the weld zone using volumetric heat flux distribution functions. Fourthly, the evolution of the structural response has been tackled through a stepwise non-linear coupled analysis. The numerical simulations are validated by means of full-scale experimental welding tests on stainless steel plates. Finally, the results and conclusions of this research work are exposed.

Keywords: Welding process; distortion; modelling; FEM; temperature-dependent properties.

Nomenclature

A	surface area of the body through which heat flows, m^2
$\mathbf{a}$	nodal displacements vector, m
$\bar{B}$	global strain shape function, dependent on **a**, m^{-1}
B_0	infinitesimal strain shape function, m^{-1}
B_L	large strain shape function, dependent on **a**, m^{-1}
C	specific heat, temperature-dependent, J/kg K
D	elastic constant matrix, temperature-dependent, Pa
E	Young's modulus temperature-dependent, Pa
$\mathbf{f}$	external forces vector, N
h	equivalent film coefficient, W/m^2K
K_T	total tangential stiffness matrix, N m^{-1}
K_0	small displacements stiffness matrix, N m^{-1}
K_L	large displacements stiffness matrix, N m^{-1}
K_σ	initial stress or geometric stiffness matrix, N m^{-1}
$\dot{Q}$	thermal heat source rate, W/m^2s

q_L	surface heat loss, W/m^2
q_L^c	convection surface heat loss, W/m^2
q_L^r	radiation surface heat loss, W/m^2
s_{ij}	deviatoric stress tensor $\left[= \sigma_{ij} - \left(\frac{1}{3} \sigma_{kk} \delta_{ij} \right) \right]$, Pa
t	time, s
U_x	nodal displacement in X direction, m
U_y	nodal displacement in Y direction, m
U_z	nodal displacement in Z direction, m
α_1	convective heat transfer, W/m^{2}K
α_2	radiative heat transfer, W/m^{2}K
α	temperature-dependent thermal expansion coefficient, K^{-1}
δ_{ij}	Kronecker's delta, dimensionless
ε	emissivity of the body Ω (dimensionless)
$\dot{\varepsilon}_{ij}$	strain rate tensor, s^{-1}
γ	plastic flow factor, Pa^{-1} s^{-1}
λ	material thermal conductivity, temperature-dependent, W/m K
ν	Poisson's ratio, dimensionless and temperature-dependent
θ	temperature of the studied body Ω, K
θ_a	ambient temperature, K
θ_{cut}	cut-off temperature, K
θ_f	material fusion temperature, K
θ_i	nodal temperature, K
ρ	material density, temperature-dependent, kg/m^3
$\boldsymbol{\sigma}$	stress tensor, Pa
$\dot{\sigma}_{ij}$	stress rate tensor, Pa s^{-1}
σ_e	von Mises effective stress $\left[= \sqrt{\frac{3}{2} s_{ij} s_{ij}} \right]$, Pa
σ_Y	yield stress, Pa
σ_{sb}	Stefan-Boltzmann constant [$= 5.67 \times 10^{-8}$ W/m^{2}K^4]
Ψ	sum of generalized external and internal forces, N

1. Introduction

1.1. Background

Duplex stainless steels are finding increased application in the chemical, oil and gas industries, petrochemical process plants, the pulp and paper industry, pollution control equipment, transportation and for general engineering thanks to their outstanding corrosion resistance and mechanical properties [1].

The high corrosion resistance and the excellent mechanical properties combination of duplex stainless steels can be explained by their chemical composition and balanced "duplex" microstructure of approximately equivalent volume fractions of ferrite and austenite. Firstly, the chemical composition based on high contents of Cr and Mo, improves intergranular and pitting corrosion resistance, respectively. Moreover, additions of nitrogen can promote structural hardening by an interstitial solid solution mechanism, which raises the yield strength and ultimate strength values without impairing toughness. Secondly, the two-phase microstructure guarantees higher resistance to pitting and stress corrosion cracking in comparison with conventional stainless steels [2].

Duplex stainless steels are typically twice as strong as common austenitic stainless steels. The thermal expansion in the duplex grades is intermediate to that of carbon steel and the austenitic stainless steels. The thermal conductivity in duplex stainless steels is also intermediate to that of carbon steels and the austenitic stainless steels.
Duplex stainless steels, with higher thermal conductivity and lower coefficient of thermal expansion, do not create the same high intensity of local thermal stresses at the welds of austenitic stainless steels [3].

1.2 Aim

A complex state of thermal and residual stresses is developed in a welded structure as a direct consequence of the uniform heat supplied and the subsequent cooling process, these stresses being able to reduce the load-carrying capacity of the structure. The high level of traction stresses in the neighborhood of the seam can increase the tendency to brittle fracture and can originate serious changes in stress corrosion and fatigue behavior. The residual compression stresses in connection with the associated distortions can originate local or global instability.

All of this justifies designer interest in knowledge of the residual stress state, both qualitatively and quantitatively. This knowledge would also permit a more rational and precise use of the stress-relief techniques, especially those based on a compensation of the existing residual stresses [4].

It is generally understood that welding involves highly complex phenomena, arising from interaction between thermal transients and the elastoplastic and structural responses of the assembly, together with the metallurgical transformation of the material being welded and the effects of turbulence on molten pool transport [5-6].

Following this last research trend, the main goal of this paper is to establish a set of approximations and simplifications in the numerical modeling of stainless steels welding, in order to reduce the huge computation time due to the coupled and non-linear formulations. Moreover, after reaching the above mentioned target, it is possible to tackle the different welding distortions for duplex and austenitic materials and compare them. Finally, the numerical results from the finite element model are compared with the experimental values measured in the specimens and conclusions are exposed.

2. Stainless Steel material properties and welding process parameters

The material properties of weld metal, base metal and heat affected zone are all temperature dependent. Due to the lack of information on material properties, both thermal and mechanical properties of weld metal and heat affected zone were assumed to be the same than those of the base metal in this analysis.

Fig. 1. Thermo-physical material properties for duplex and austenitic stainless steels: specific heat (left) and thermal conductivity (right).

On the one hand, at about 1,773 K the duplex steel is melted and over this value there is liquid. The LDX-2101 (EN-1.4462 according to British Standard rule [7]) thermal material properties are reported in Fig. 1. On the other hand, the austenitic stainless steel EN-1.4404 [7] is melted about 1,573 K. From the above database it is not possible to know the material properties in the liquid phase, and the unique way at this stage is to keep the physical properties constant outside the solid range. The temperature-dependent mechanical properties for duplex and austenitic stainless steels used in the simulation are shown in Fig. 2.

Fig. 2. Mechanical material properties for duplex and austenitic stainless steels: (a) yield strength, (b) ultimate tensile strength, and bilinear piece wise tensile-elongation relationship for different temperatures: (c) duplex steel and (d) austenitic steel.

The amount of heat input for both stainless steels were found as the product of arc efficiency, voltage, current and welding speed, as it is shown in Table 1. The total net heat input was assigned to the weld metal as uniform body loads.

Table 1
Welding parameters

3. Mathematical model

In order to build accurate numerical models of welding, we are going to consider all the parameters of the process (number and sequence of steps, welding speed, etc.), material nonlinearities, geometrical constraints, and all physical phenomena involved in welding following the previous work by Capriccioli and Frosi [8]. In this sense, it is a great daring to take into account all the important factors of the welding process at the same time. Therefore, this research work assumes the following main hypotheses and characteristics about the thermal model [8-10]:

- Radiation and convection effects have been considered here.
- All the material properties are described till the liquid metal phase.
- During the welding process, the displacement of the parts does not affect the thermal distribution of the parts themselves.
- The birth and death technique has been used [8] to simulate the material deposition, as it is explained in subsection 3.3.

The weldment thermo-mechanical behaviour during the welding process is simulated using uncoupled formulation, because the dimensional changes in welding are negligible and the mechanical work done is insignificant compared to the thermal energy from the welding arc. Therefore, an uncoupled thermal and thermo-mechanical analysis is adopted in this work [9-11]. In the first place, a thermal analysis was carried out in the first step and during this phase the temperatures distributions are calculated and saved for every load step. In the second place, the transient temperature outputs from the previous analysis are used for a thermo-mechanical subsequent analysis. It is assumed that the thermal calculation at a given time is independent from the structural results obtained at a previous time according to the first hypothesis. Thus, the thermal and mechanical analyses can be uncoupled [8-11].

The heat conduction problem is solved independently from the stress problem to obtain the temperature history. However, the formulation considers the contributions of the transient temperature field to the stress analysis through thermal expansion, as well as temperature-dependent thermo-physical and mechanical properties [8]. The solution procedure consists of two steps. First, the temperature distribution and its history in the welding model are computed by the heat conduction analysis. Then, the temperature history is employed as a thermal load in the subsequent mechanical elastoplastic calculation of the residual stress field.

3.1. Thermal analysis

In the thermal analysis, the transient temperature field θ in the molten weld pool is a function of time *t* and the spatial coordinates $\left(x, y, z\right)$ and is assumed to be governed by the same equation as the applied to the solid metal region. The governing partial differential equation for transient heat conduction, with internal heat generation, is given by the thermal equilibrium equation; that is to say, it is determined by the following three-dimensional nonlinear heat transfer equation [11-16]:

$$\lambda\left(\theta\right)\left\{\frac{\partial^2\theta}{\partial x^2}+\frac{\partial^2\theta}{\partial y^2}+\frac{\partial^2\theta}{\partial z^2}\right\}+\dot{Q}=\rho\left(\theta\right)C\left(\theta\right)\frac{\partial\theta}{\partial t} \tag{1}$$

It is important to take into account that the heat flux to the system is input by a moving source on the boundary.

Therefore, the materials are melted over 1,773 K and 1,573 K (see section two/2). In order to simulate the phase change we have used the enthalpy formulation ($\Delta H=\int\rho\left(\theta\right)C\left(\theta\right)d\theta$). This function depends on the previous values of density ρ and specific heat *C* at the same temperature [8]. The integration arbitrary constant is assumed equal to the product $\rho C\theta$ at 273 K (0ºC). In this way, at the solidus temperature, it is necessary to add the latent heat to obtain the enthalpy value at the liquidus temperature. Therefore, it is possible to model with only one material parameter the whole thermal history including heat exchange during solidification or melting. In the liquid phase, the parameters *C* and ρ are assumed constant, so that the enthalpy in that interval has a constant slope given by the last values defined for *C* and ρ.

Surface heat flow, that can take place into or from the model during the processes cited above, is specified by the following boundary conditions [11]:

- Surface heat input condition through rate of heat input for unit surface area q_I (applicable for welding to model the energy input from weld electrode).
- Surface heat loss due to convection and radiation:

$$q_L = q_L^c + q_L^r = \alpha_1(\theta-\theta_a) + \alpha_2(\theta-\theta_a) = (\alpha_1+\alpha_2)(\theta-\theta_a) \tag{2}$$

Heat loss from the surfaces at temperatures near the melting point to ambient is predominantly due to radiation, and is given by [9-11]:

$$q_L^r = \varepsilon\sigma_{sb}A\left(\theta^4-\theta_a^4\right) = \left[\varepsilon\sigma_{sb}A\left(\theta^2+\theta_a^2\right)\left(\theta^2-\theta_a^2\right)\right] = \alpha_2(\theta-\theta_a) \tag{3}$$

Therefore, in order to consider heat convection and radiation on the plate surfaces, the heat flux loss is evaluated by the following expression [11,17]:

$$q_L = \alpha_1(\theta-\theta_a) + \varepsilon\sigma_{sb}A\left(\theta^4-\theta_a^4\right) = h(\theta)(\theta-\theta_a) \tag{4}$$

where $h(\theta)$ is given by:

$$h(\theta) = \alpha_1+\alpha_2 = \alpha_1 + \varepsilon\sigma_{sb}A(\theta+\theta_a)\left(\theta^2+\theta_a^2\right) \tag{5}$$

In this calculation, for the duplex stainless steel plates, $h(\theta)$ W/m^{2}K is obtained through our experimental tests. In addition, a fusion latent heat of 500 J/kg K is taken in order to consider the phase transformation of this steel. This last value was obtained from the Outokumpu product specification data and other previous research works [18]. With respect to the austenitic stainless steel, a fusion latent heat of 330 J/kg K is used in order to consider its phase transformation [19].

The variational formulation of this problem permits that the surface boundary conditions stated above may be treated implicitly together with the equilibrium equation. In this sense, the solution is obtained applying the *principle of virtual temperatures* [11-17].

3.2. Mechanical analysis

3.2.1. Plasticity

On the one hand, the plastic strain in both types of stainless steels fulfil the Von Mises yield criterion with isotropic strain hardening as well as its corresponding associated flow rule. Further, we have chosen the bilinear isotropic plasticity to model both types of steels. The rate relationship of different components between thermal stresses, $\boldsymbol{\sigma}$, and strains, $\boldsymbol{\varepsilon}$, is given by the following expression [9-10]:

$$\dot{\varepsilon}_{ij} = \frac{1+\nu}{E}\dot{\sigma}_{ij} - \frac{\nu}{E}\dot{\sigma}_{kk}\delta_{ij} + \gamma s_{ij} + \left[\alpha + \frac{\partial\alpha}{\partial\theta}(\theta-\theta_a)\right]\frac{\partial\theta}{\partial t} \tag{6}$$

Furthermore, it is well known that $\sigma_e < \sigma_Y$ for elastic deformation ($\gamma = 0$) and $\sigma_e \geq \sigma_Y$ for plastic deformation ($\gamma > 0$).

On the other hand, in our structural thermo-mechanical analysis, a cut-off temperature around 2/3 of the melting temperature (see sub-section 4.3, entitled Mechanical analysis) is used in the numerical calculations to reduce unnecessary computational time

[5]. To save computational time without losing accuracy of results, different time steps are used for the two analyses. The initial time steps used in this study are 0.15s and 30s for the heat transfer analysis (heating and cooling phases respectively), and 0.2s and 15s for the stress-strain analysis (heating and cooling phases respectively). As such, the CPU time in a typical welding simulation is about 18min for the temperature computation and 256min for stress-strain computation in a welded seam between two plates whose size is $300\times200\times3\,\text{mm}$ (length, width and thickness, respectively). The numerical models have been solved on a workstation computer with a CPU Intel Core2 Quad Q6600, 8 GB RAM memory and 4.5 TB hard disk. The total elapsed CPU average time for each model was 274min.

3.2.2. Large displacements

In many problems it has been implicitly assumed that both displacements and strains developed in the structure are small. In practical terms this means that the geometry of the elements remains basically unchanged during the loading process and that first-order, infinitesimal, linear strain approximations can be used.

In practice such assumptions fail frequently even though actual strains may be small and elastic limits of ordinary structural materials are not exceed. If accurate determination of the displacements is needed, geometric non-linearity may have to be considered in some structures [20-21]. Conversely, it may be found that a load is reached where deflections increase more rapidly that predicted by a linear solution and indeed a state may be attained where load-carrying capacity *decreases* with continuing deformation. This classic problem is that of structural stability and obviously has many practical implications. The applications of such an analysis are clearly of considerable importance in aerospace engineering, design of radio telescopes, cooling towers, box girders bridges and other relatively slender structures. In many cases *very large displacements* may occur without causing large strains. Typical in this context is the classical problem of the ‘elastica’ of which an example is a watch spring.

Whether the displacements (or strains) are large or small, equilibrium conditions between internal and external ‘forces’ have to be satisfied. Thus, if the displacements are prescribed in the usual manner by a finite number of nodal parameters $\mathbf{a}$, we can obtain the necessary equilibrium equations using the *virtual work principle* [12-14,20]:

$$\Psi(\mathbf{a}) = \int_{\Omega} \bar{B}^T \boldsymbol{\sigma}\, d\Omega - \mathbf{f} = 0 \tag{7}$$

in which $\bar{B}$ is defined from the strain definition $\boldsymbol{\varepsilon}$ as:

$$d\boldsymbol{\varepsilon} = \bar{B}\, d\mathbf{a} \tag{8}$$

The bar suffix has now been added for, if displacements are large, the strains depend non-linearly on displacement, and the matrix $\bar{B}$ is now dependent on $\mathbf{a}$. We see that it can be conveniently written [20]:

$$\bar{B} = B_0 + B_L(\mathbf{a}) \tag{9}$$

in which B_0 is the same matrix as in linear infinitesimal strain analysis and only B_L depends on the displacement. In general, B_L will be found to be a *linear function* of such displacements.

Clearly, the solution of Eq. (7) will have to be approached iteratively. If, for instance, the Newton-Raphson process is to be adopted we have to find the relation between $d\mathbf{a}$ and $d\Psi$. Thus taking appropriate variations of Eq. (7) with respect to $d\mathbf{a}$ we have [20]:

$$d\Psi = \int_{\Omega} d\bar{B}^T\, \boldsymbol{\sigma}\, d\Omega + \int_{\Omega} \bar{B}^T\, d\boldsymbol{\sigma}\, d\Omega = K_T\, d\mathbf{a} \tag{10}$$

and using equation $d\boldsymbol{\sigma} = D\, d\boldsymbol{\varepsilon}$ and Eq. (8) it is obtained:

$$d\boldsymbol{\sigma} = D\, d\boldsymbol{\varepsilon} = D\, \bar{B}\, d\mathbf{a} \tag{11}$$

and taking into account the Eq. (9), it is verified that $d\bar{B} = dB_L$. Therefore,

$$d\Psi = \int_{V} dB_L^T\, \vec{\sigma}\, dV + \bar{K}\, d\vec{a} = K_\sigma\, d\vec{a} + \bar{K}\, d\vec{a} \tag{12}$$

where

$$\bar{K} = \int_{V} \bar{B}^T D\, \bar{B}\, dV = K_0 + K_L \tag{13}$$

in which K_0 and K_L are given by [12, 20]:

$$K_0 = \int_{V} B_0^T\, D\, B_0\, dV\,, \qquad K_L = \int_{V} \left(B_0^T\, D\, B_L + B_L^T\, D\, B_L + B_L^T\, D\, B_0 \right) dV \tag{14}$$

To summarize, Eq. (12) can be expressed globally as [20]:

$$d\Psi = \left(K_0 + K_\sigma + K_L \right) d\mathbf{a} = K_T\, d\mathbf{a} \tag{15}$$

Newton-type iteration can be once more applied precisely in order to solve the final non-linear problem.

3.3. Birth and death technique

If material is added to a system, certain elements in the FEM model may become *existent*. In such cases, it is possible to use element birth and death technique to deactivate or reactivate some finite elements. In this paper, to simulate the filling deposition of TIG welding procedure, the previous technique is chosen [8].

These elements are collected in groups according to the torch's movement, as it is shown in Fig. 3. To achieve the "element death" effect, the numerical procedure does not actually remove "killed" elements. Instead, it deactivates them by multiplying their stiffness by a reduction factor of 1.0×10^{-6} [22].

In the first place, the elements describing the molten material are selected and deactivated. Next, they are reactivated in the thermal analysis according to the actual welding speed of the TIG manufacturing process.

Fig. 3. Element birth and death sequence in the TIG welding process.

Elements loads associated with deactivated elements are zeroed out of the load vector. In case of the TIG welding procedure, the deactivated elements mass and energy are not considered. Furthermore, the element's strain is also set to zero as soon as that element is killed. When the elements are activated, the heat input generation is applied as a load in the thermal FEM model, and the thermal strains are computed for newly-activated elements based on the current load step temperature and the reference temperature.

4. Finite element analysis

Welding processes are very difficult to model due to the complicated physics involved, which includes phenomena such as fluid mechanics with phase changes, shrinkage and porosity, macrosegregation among others. Each of the phenomena is a subject of intense research [5,8,23-24]. Taking into consideration even a few of these phenomena simultaneously can make welding analysis an extremely difficult problem. To make numerical simulation of welding, a number of simplification assumptions have to be made.

The present research paper deals with a finite element analysis that was carried out in two steps. A non-linear transient thermal analysis was conducted first to obtain the global temperature history generated during the welding and cooling processes. Then, a structural analysis was developed with the temperatures obtained from the thermal analysis used as loading to the stress model. The advantage of a decoupled approach is computational simplification and efficiency.

Because of the thermo-mechanical nature of welding process theoretical considerations can be assessed either using a thermal or a mechanical analysis. Welding thermal stresses are calculated from the temperature distributions determined by the thermal model. The residual stresses from each temperature increment are added to the nodal point location to determine the updated behaviour of the model before the next temperature increment.
A simplified flowchart corresponding to the numerical analysis is shown in Fig. 4.

Fig. 4. Flowchart corresponding to the numerical analysis.

Welding in large unrestrained structures can cause significant distortions in modes that simplified two dimensional analyses of the weld region may not capture. Specifically, the parts may move relatively to each other, and the weld may be placed in a different location than that of the undeformed configuration, for these reasons, in this simulation, a three dimensional finite element analysis was used to simulate the welding process.

4.1. Finite element meshing

The mesh used in the stress analysis was identical to that in the thermal analysis. Fig. 5 shows the entire FEM model of the butt weld. To increment the computer efficiency, three zones with different mesh densities are used. The finest mesh corresponds with the 'fusion zone', whereas the coarsest corresponds with the 'base metal'. Between them, a transition mesh was imposed with a properly element size which matches the 'heat affected zone'.

Fig. 5. Entire FEM model of the butt weld.

Eight-node brick elements with linear shape functions are used in the model meshing. For thermal analysis, the element type is SOLID70 which has single degree of freedom, temperature, on its each node. For structural analysis the element type is SOLID185 with three translational degrees of freedom at each node [22].

4.2. Thermal analysis

The heat source movement has been simulated with a thermal load applied to the elements that represent the fused material at a given time. The birth and death technique has been used. Figs. 3 and 5 show the finite elements that simulate the filling material, these elements are removed at the beginning of the thermal analysis and then, for every load step, a cross sectional strip of elements are activated and loaded to simulate the passage of the heat source and the filling material deposition. The arc heat input was applied in the welding zone using a piecewise volumetric heat flux distribution function.

Thermo-fluids phenomena are neglected in this direct approach, and conduction, convection and radiation are simulated and the thermo-physical characteristics are considered as temperature dependent. On the one hand, the effect of latent heat of fusion is taken into account by use of an enthalpy method. On the other hand, it is assumed that the thermal conductivity is constant after melting, whose value is three times that corresponding to this melting temperature (see Fig. 1 lower).

In the thermal analysis, a total of 33 load steps with a maximum of 23 sub-steps and a minimum of 5 sub-steps were required to complete the heating cycle. Automatic time stepping and full Newton-Raphson method were used in each time step for the heat balance iteration.

4.3. Mechanical analysis

The material elastic–plastic behaviour has been implemented in the finite element code using a piece-wise linear fit to the true stress–plastic strain curves. The simplified model is presented in Figs. 2c and 2d for duplex and austenitic stainless steels, respectively. Rate-independent plasticity is modelled using the incremental theory with a von Mises yield surface, associated flow rule and isotropic hardening. The convergence´s problems coming from the small tangent modulus at high temperature can be overcome using a meshing parameter of 2mm value and activating seven axial elements for a single drop in the welding zone. The material is assumed to present zero stiffness for temperatures exceeding a specified temperature, named "cut-off" temperature. Above this temperature any thermal strain is not considered [5].

Moreover, the effect of specifying different cut-off temperatures has been investigated, as it is indicated in Table 2. Fig. 6 shows the effect of the cut-off temperatures variation in the maximum vertical displacement as well as the total CPU time for both stainless steels.

On the one hand, a numerical convergence problem can occur when the cut-off temperature increases, as it is possible to see in the total CPU time graph. The origin of this numerical problem can be explained by the appearance of excessive distortions due to a huge reduction of the material stiffness for such high temperatures. On the other hand, when the cut-off temperature is varied in the range considered in this study (see Table 2), a maximum vertical displacement is obtained. Consequently, the cut-off temperature values shown in Table 2 are used in the subsequent numerical calculations.

Fig. 6. Cut-off temperature effects for both stainless steels: total CPU time (left) and maximum vertical displacement (right).

As it is shown in Fig. 7, the data from the temperature field is applied via a loop comparing the nodal temperature in all nodes for each time step. If the nodal temperature is greater than the cut-off temperature, then the temperature in this node is fitted to this value. Once all nodal temperatures are defined, the non-linear, stepwise static structural analysis is solved for current time step until all elements of the model have been activated.

Fig. 7. Flowchart corresponding to the structural analysis

5. Results and discussion

In order to check the numerical results obtained from the finite element model, several experimental measurements have been made. Simple criteria have been followed to develop the testing methodologies. These methodologies are very useful to validate the simulation tool from a practical point of view. All of them and the main results obtained with the corresponding comparisons are explained as follows.

5.1. Experimental and numerical thermal results

To validate the numerical results of the thermal analysis, a set of thermographies have been taken at different times. In this way, a sequence of the different thermal states of the piece along the welding process can be observed.

The thermographic principle is based on capturing infrared emission from the subject under investigation. For this purpose, a FLIR ThermaCAM™ E2 thermographic camera with a focal plane detector type (array of 160×120 pixels) has been employed. This device captures infrared radiation at wavelengths in the range of 7.5 to 13μm and temperatures ranging from 253 to 523 K. The accuracy of the measured temperature is ±2K and the value adopted for the material emissivity was 0.85 [25]. The thermographies were taken at a focus distance of 1m.

It is possible to directly compare the pictures obtained from the thermographic camera with the thermal fields obtained from the numerical analysis at each step of the process. Fig. 8. shows the results at the following time steps: 274s, 780s, and 1,300s, respectively.

Fig. 8. Comparison between experimental thermographies (left, a, c, e) and numerical results (right, b, d, f).

Fig. 8 also shows the comparison between numerical and experimental results for different time steps. A good agreement is observed for the temperature fields in several locations. The small differences are due to material emissivity changes, caused by the variation of the temperature field and surface texture during the welding process. However, the maximum and minimum temperature values are a very close match.

5.2. Experimental measurements and structural analysis results

The results of the structural analysis are the practical and main purpose of this work. From this analysis it is possible to find out the stress, strains and displacements in both plates and weld pool when they are subject to a suddenly thermal process as welding.

In order to validate the numerical FEM displacements, a DEA Global coordinate measurement machine (CMM) type 09.15.08 has been used (see Fig. 9). The main technical characteristics of this device are the following:

- Measuring range: 900 × 1,500 × 800mm in X, Y and Z directions.
- Accuracy: from 1.4 to maximum length divided by 333µm (1µm in this case).

Fig. 9. Experimental setup of the coordinate measuring machine (CMM): overall view (left) and a detail (right).

Fig. 10 shows a set of pictures corresponding to the deformed shape of the plates after being welded compared with the numerical results explained here.

Fig. 10. Comparison between the experimental deformed shape (left, a, c, e, g) and the numerical results (right, b, d, f, h).

In order to validate the structural analysis, vertical displacements at nine different locations have been measured over a plate. These locations correspond to three transversal sections of the plate (two of them in the vertex and the others in the middle) and, over each of them, at three distances from the weld pool (see Fig. 11).

Fig. 11. Geometrical description of the locations considered for results comparison.

The numerical method developed in the current work helps to study the evolution of the welded plates’ displacements. As in a common numerical simulation, it is possible to use two different ways of post-processing:

- Post-I: Results at specific points in the model over all time steps.
- Post-II: Overall model results at a specific time.

Fig. 12. Vertical displacement evolution at nine different locations for both specimens: duplex stainless steel plates (left) and austenitic stainless steel (right).

With the basis of Post-I procedure, Fig. 12 shows the vertical displacement evolution at the previously described locations during the whole welding process for both materials considered: duplex and austenitic stainless steels. It is possible to observe that the absolute value for the maximum vertical displacement is similar for both steels but the sign is opposite. This means that the overall deformations of the welded plates are opposite for these two materials, as it was well observed in the experimental tests.

Fig. 13. Numerical FEM displacement results for duplex (left) and austenitic (right) stainless steels in three different time steps.

Through a combination of both types of post-processing methods it is possible to compare experimental and numerical results. On the one hand, with the Post-II procedure, vertical displacements at the selected locations at the final instant of the cooling stage are obtained. On the other hand, the displacement values at these locations were experimentally obtained by means of the CMM previously indicated. The numerical and experimental comparison is shown in Fig. 14. A very good agreement between them is obtained.

Fig. 14. Comparison between vertical displacement values at selected locations for duplex (left) and austenitic (right) stainless steel. Numerical simulation vs experimental results.

6. Conclusions

Firstly, a computer code is developed for transient thermal and thermo-elasto-plastic stress coupled analyses considering various important nonlinearities due to temperature-dependent material properties. Secondly, the methodology was verified through comparison with experimental tests for different stainless steels. Thirdly, from this research work, it is possible to conclude that:

- The finite element method including the birth and death technique is an efficient procedure to analyze the vertical displacement evolution at different plate locations in the welding process of stainless steels, as well as their angular deformation and longitudinal bending.
- The use of thermographic imaging in the context of TIG welding has been successfully demonstrated on a practical scale and helps to compare the thermal results in the subsequent numerical simulation at different locations and a specific time. The maximum and minimum temperature values in the numerical simulation and the experimental setup are a very close match.
- The experimental setup of the coordinate measuring machine is appropriate to quantify vertical displacements in the welding plates at different locations. The numerical and experimental comparison shows a very good agreement between them.
- The effect of specifying different cut-off temperatures has been investigated and the effect in the total CPU time and the maximum vertical displacement was calculated. As final conclusion, the optimum value in the calculations for this

parameter was about 2/3 of the fusion temperature, specifically 1,173 K (for duplex steel) and 1,073 K (for austenitic steel).

- This paper shows the important influence of the material properties in the final deformed shape of two different stainless steels, noting that opposite angular deformation and longitudinal bending occur when these steels are welded with a similar TIG procedure.
- Finally, the methodology developed here can be applied to other types of welding processes and other different materials with success.

Acknowledgements

The authors wish to acknowledge the partial financial support provided by the Spanish Ministry of Science and Innovation grant nº BIA2008-00065. Also, they want to express deep gratitude to Mr. Jesus Gonzalez of Outokumpu Company Ltd. for their useful assistance. We also thank Swanson Analysis Inc. for the use of the ANSYS Academic program and the anonymous referee’ interesting comments and suggestions to improve the paper.

References

[1] S. Azuma, K. Ogawa, Duplex stainless steel excellent in corrosion resistance, Applied Thermal Engineering 18 (6) (1998) pp XXIV.

[2] I. Álvarez-Armas, S. Degallaix-Moreuil, Duplex Stainless Steel, Wiley-ISTE, 2009.

[3] R. Cunn, DDS Microstructure, properties and applications, Woodhead Publishing, 1997.

[4] J. Cañas, R. Picón, F. París, A. Blazquez, J. C. Martín, A simplified numerical analysis of Residual stresses in aluminum welded plates, Computers & Structures, 58 (1) (1996) 59-69.

[5] D. Camilleri, P. Mallicone, T. G. F. Gray, Alternative numerical techniques for distortion of thin plate due to fillet-welded stiffeners, Modelling and Simulation in Material Sciences and Engineering, 14 (2006) 1307-1327.

[6] N. Chakraborty, The effects of turbulence on molten pool transport during melting and solidification processes in continuous conduction mode laser welding of copper–nickel dissimilar couple, Applied Thermal Engineering, 29, (17-18) (2009) 3618-3631.

[7] BS EN-1995-1-2:1995. Design of steel structures. Part 1-2: General rules-Structural fire design. British Standard Institute, London, 2006.

[8] A. Capriccioli, P. Frosi, Multipurpose ANSYS FE procedure for welding processes simulation, Fusion Engineering and Desing, 84 (2009) 546-553.

[9] X.K. Zhu, Y.J. Chao, Effects of temperature-dependent material properties on welding simulation, Computers & Structures, 80 (2002) 967-976.

[10] X.K. Zhu, Y.J. Chao, Numerical simulation of transient temperature and residual stresses in friction stir welding of 304L stainless steel, Journal of Materials Processing Technology, 146 (2004) 263-272.

[11] Y.V.L.N. Murthy, G. Venkata Rao, P. Krishna Iyer, Numerical simulation of welding and quenching processes using transient thermal and thermo-elasto-plastic formulations, Computers & Structures, 60 (1) (1996) 131-154.

[12] K. Bathe, Finite Element Procedures, Prentice-Hall, Englewoods Cliffs, New Jersey, 1998.

[13] R. D. Cook, D. S. Malkus, M. E. Plesha, R. J. Witt, Concepts and Applications of Finite Element Analysis, Wiley, New York, 2001.

[14] T. Chandrupatla, A. Belegundu, Introduction to Finite Element in Engineering, Englewood Cliffs, Prentice-Hall, New Jersey, 1991.

[15] A.F. Mills, Heat Transfer, Prentice Hall, New York, 1998.

[16] J. J. del Coz Diaz, P. J. Garcia Nieto, J. L. Suarez Sierra, C. Betegon Biempica, Nonlinear thermal optimization of external light concrete multi-holed brick walls by the finite element method, International Journal of Heat and Mass Transfer, 51 (7-8) (2008) 1530-1541.

[17] R. Siegel, J. R. Howell, J. Howell, Thermal Radiation Heat Transfer, Taylor & Francis Group, 2001.

[18] A. Pilipenko, Computer simulation of residual stress and distortion of thick plates in multi-electrode submerged arc welding. Their mitigation techniques. Ph. D thesis. Department of Mach. Designing and Material Technology, Norwegian University of Science and Technology, 2001.

[19] L-E. Lindgren, L. Karlsson, Deformations and stresses in welding of shell structures, INternational Journal for Numerical Methods in Engineering, 25 (1988) 635-655.

[20] O. C. Zienkiewicz, R. L. Taylor, The Finite Element Method, McGraw-Hill Book Company, United Kingdom, 1991.

[21] J. J. del Coz Diaz, P. J. Garcia Nieto, M. Fernandez Rico, J. L. Suarez Sierra, Non-linear analysis of the tubular 'heart' joint by FEM and experimental validation, Journal of Constructional Steel Research, 63 (8) (2007) 1077-1090.

[22] E. Madenci, I. Guven, The Finite Element Method and Applications in Engineering using ANSYS, Springer, Berlin, 2005.

[23] V. S. Sergey, S. Paolucci, Numerical simulation of filling and solidification of permanent mold castings, Applied Thermal Engineering, 22(2) (2002) 229-248.

[24] N. Pathak, A. Kumar, A. Yadav, P. Dutta, Effects of mould filling on evolution of the solid–liquid interface during solidification, Applied Thermal Engineering 29 (17-18) (2009) 3669-3678.

[25] W. L. Wolfe, G. J. Zissis, The Infrared Handbook, Office of Naval Research, Department of Navy, Washington D.C., 1985.

Table 1
Welding parameters

Item	Units	Duplex steel EN-1.4462	Austenitic steel EN-1.4404
Welding process efficiency	%	75	85
Voltage	V	23	13
Current intensity	A	180	115
Welding speed	m/s	1.67×10^{-3}	4.8×10^{-3}

Table 2
Cut-off temperatures determination

Item	θ_f [K]	θ_{cut} [K]	Ranging cut-off temperatures [K]
Duplex stainless steel	1,773	1,173	1,073 to 1,273
Austenitic stainless steel	1,573	1,073	973 to 1,173

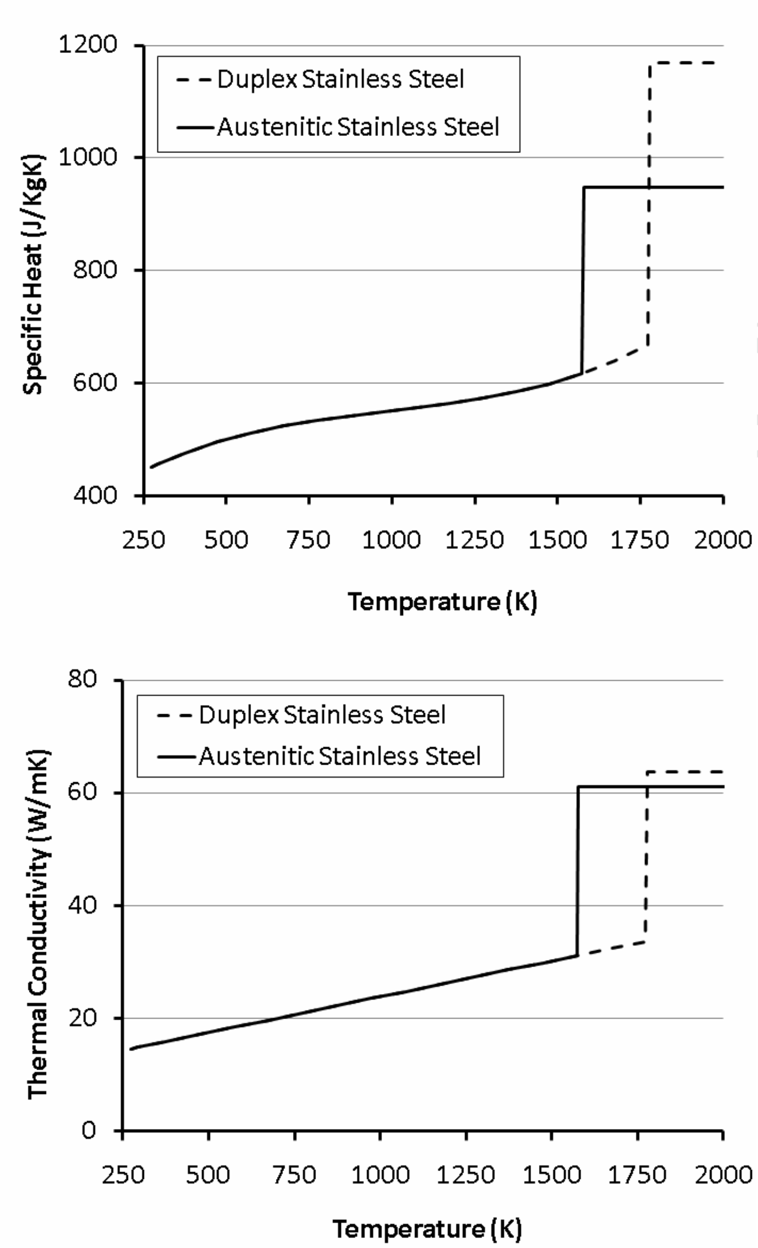

Fig. 1. Thermo-physical material properties for duplex and austenitic stainless steels: specific heat (upper) and thermal conductivity (lower).

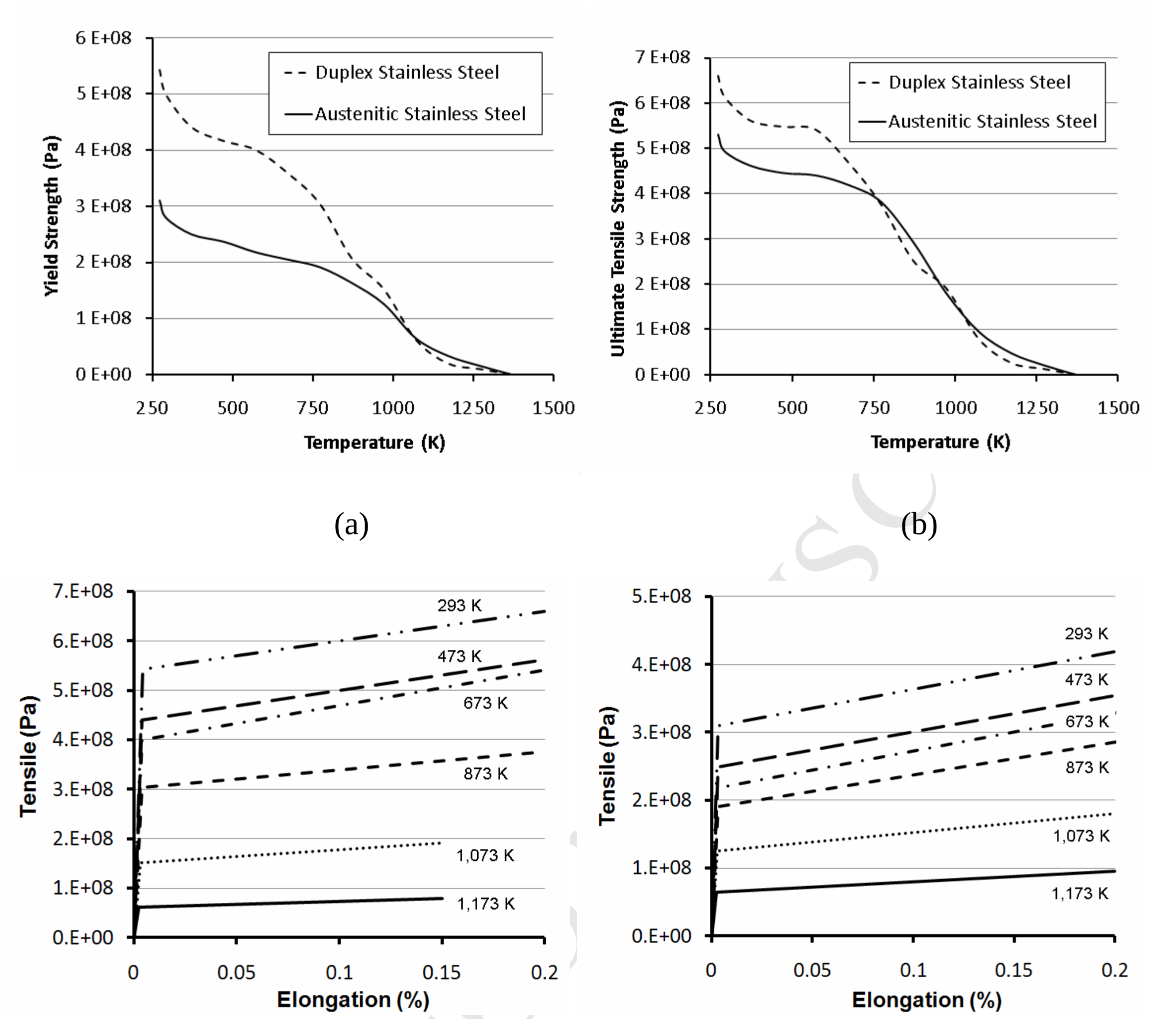

(a) (b)

(c) (d)

Fig. 2. Mechanical material properties for duplex and austenitic stainless steels: (a) yield strength, (b) ultimate tensile strength, and bilinear piece wise tensile-elongation relationship for different temperatures: (c) duplex steel and (d) austenitic steel.

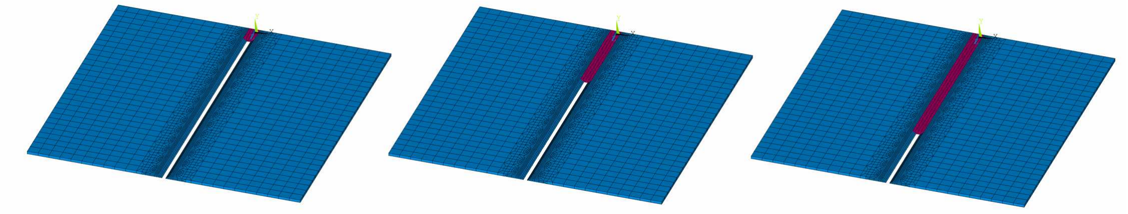

Fig. 3. Element birth and death sequence in the TIG welding process.

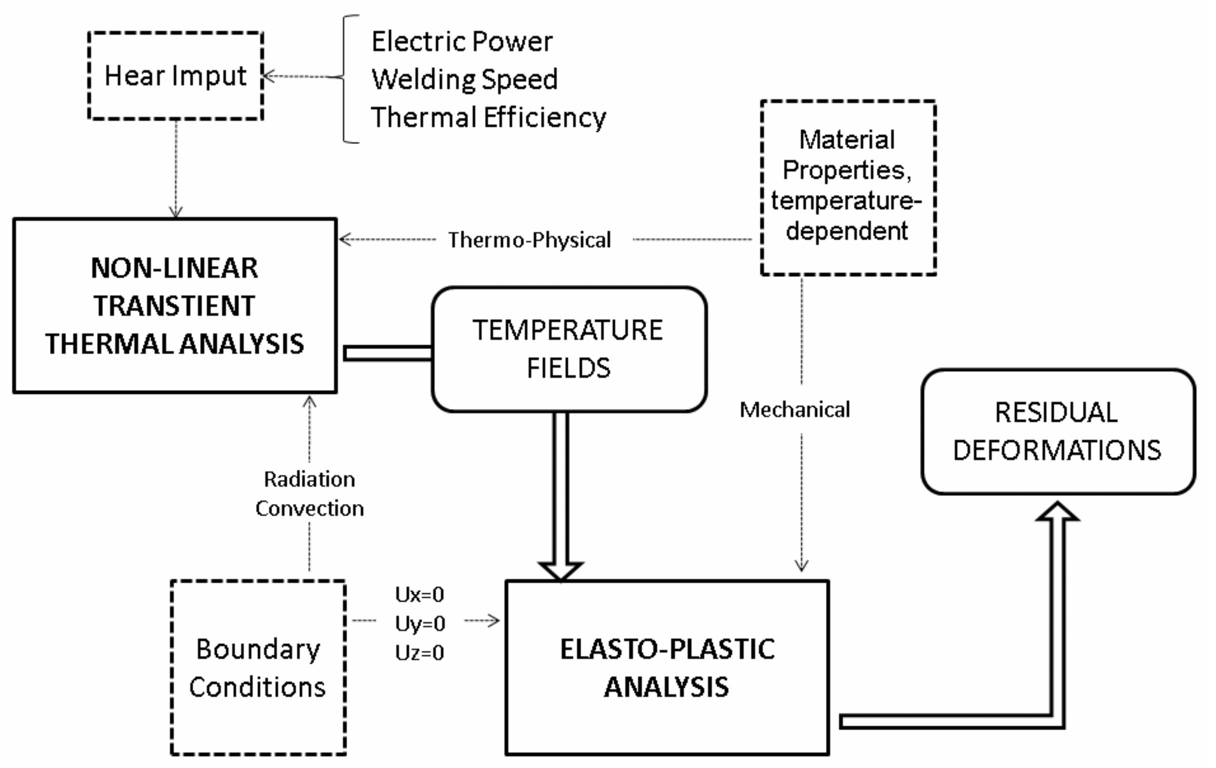

Fig. 4. Flowchart corresponding to the numerical analysis.

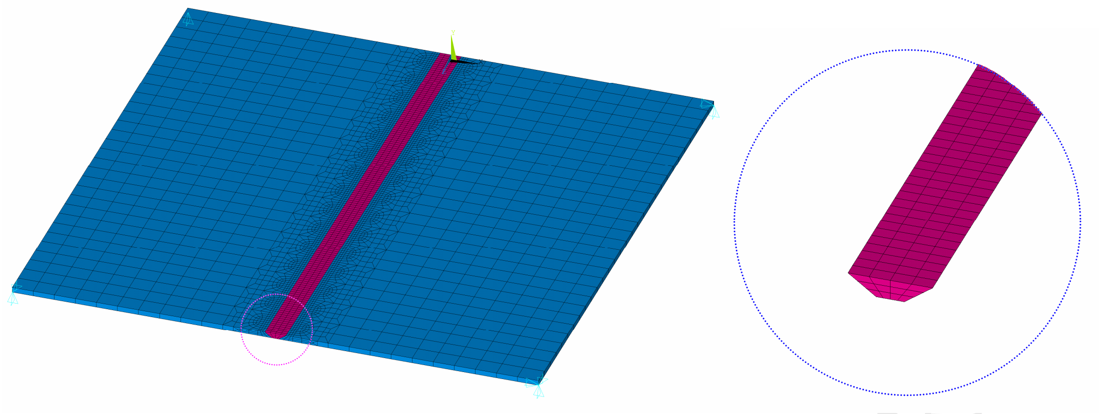

(a) Complete model of the butt weld. (b) Detail of the filler elements.

Fig. 5. Entire FEM model of the butt weld.

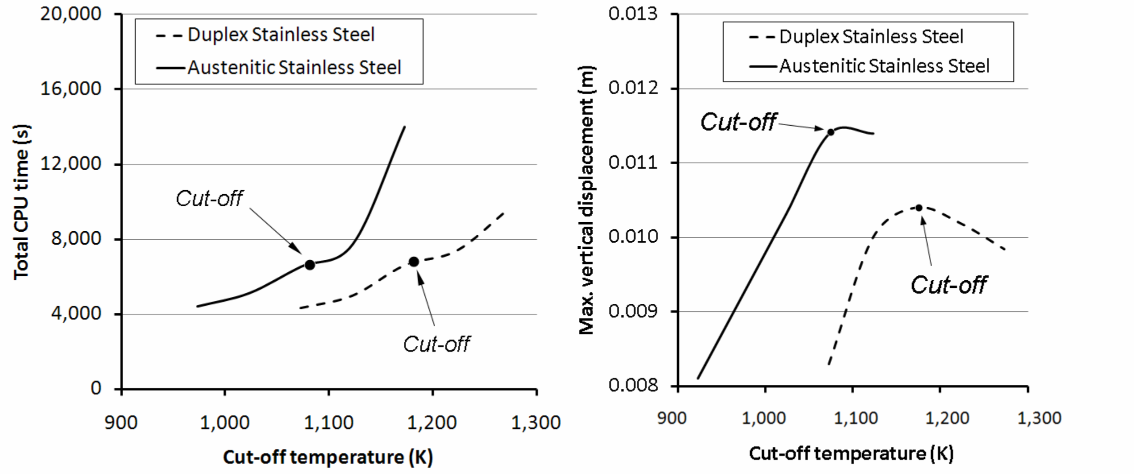

Fig. 6. Cut-off temperature effects for both stainless steels: total CPU time (left) and maximum vertical displacement (right).

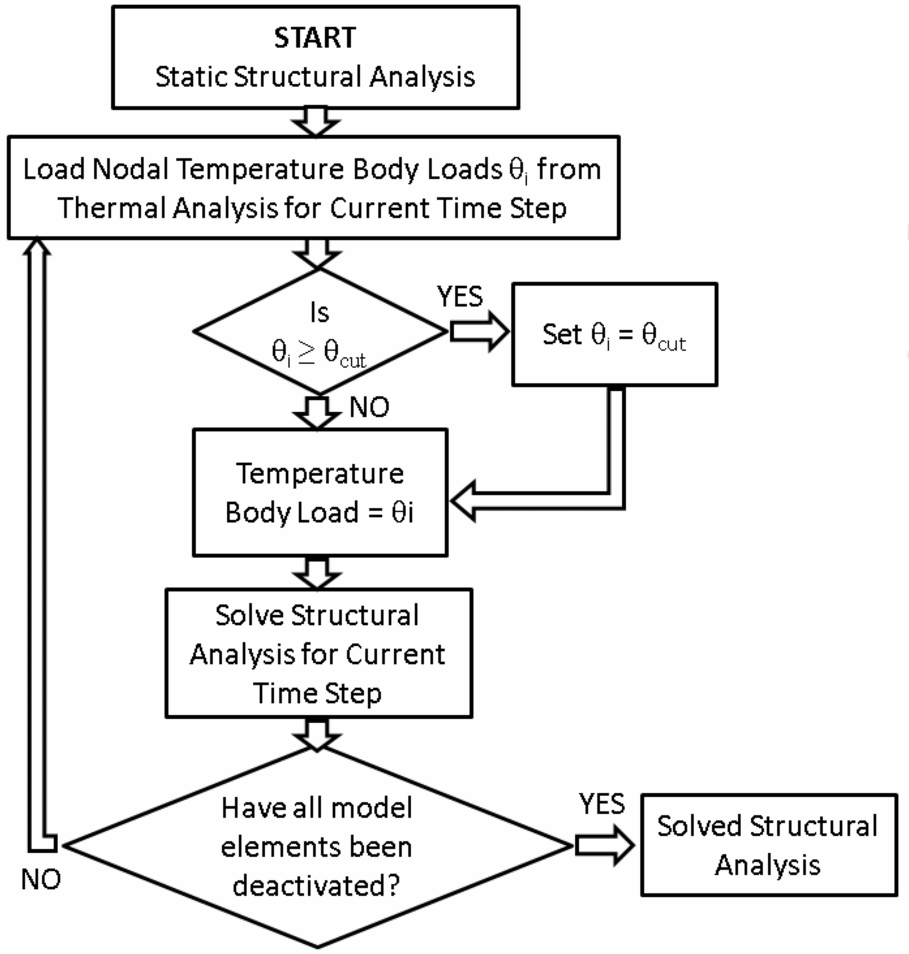

Fig. 7. Flowchart corresponding to the structural analysis.

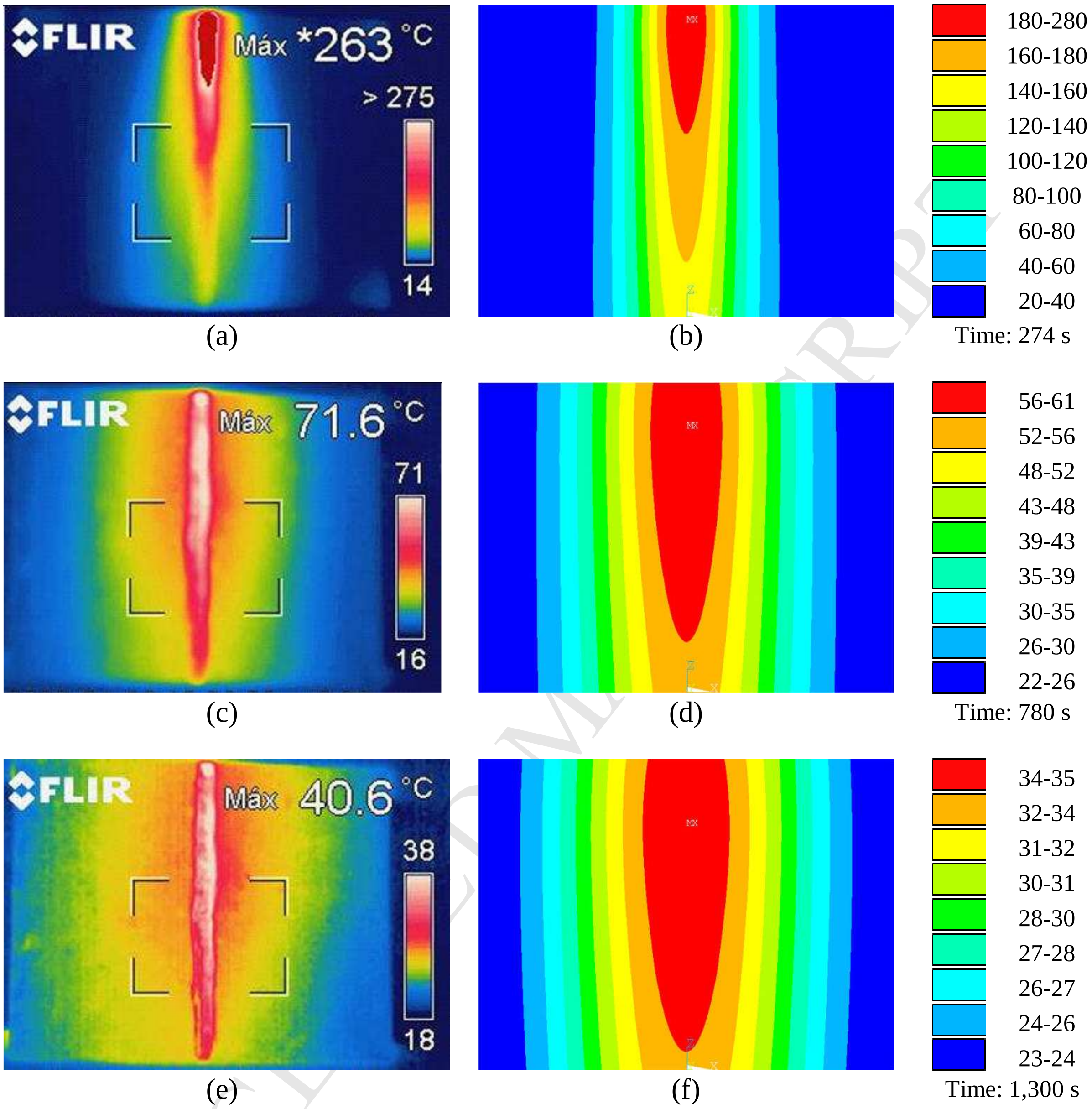

Fig. 8. Comparison between experimental thermographies (left, a, c, e) and numerical results (right, b, d, f).

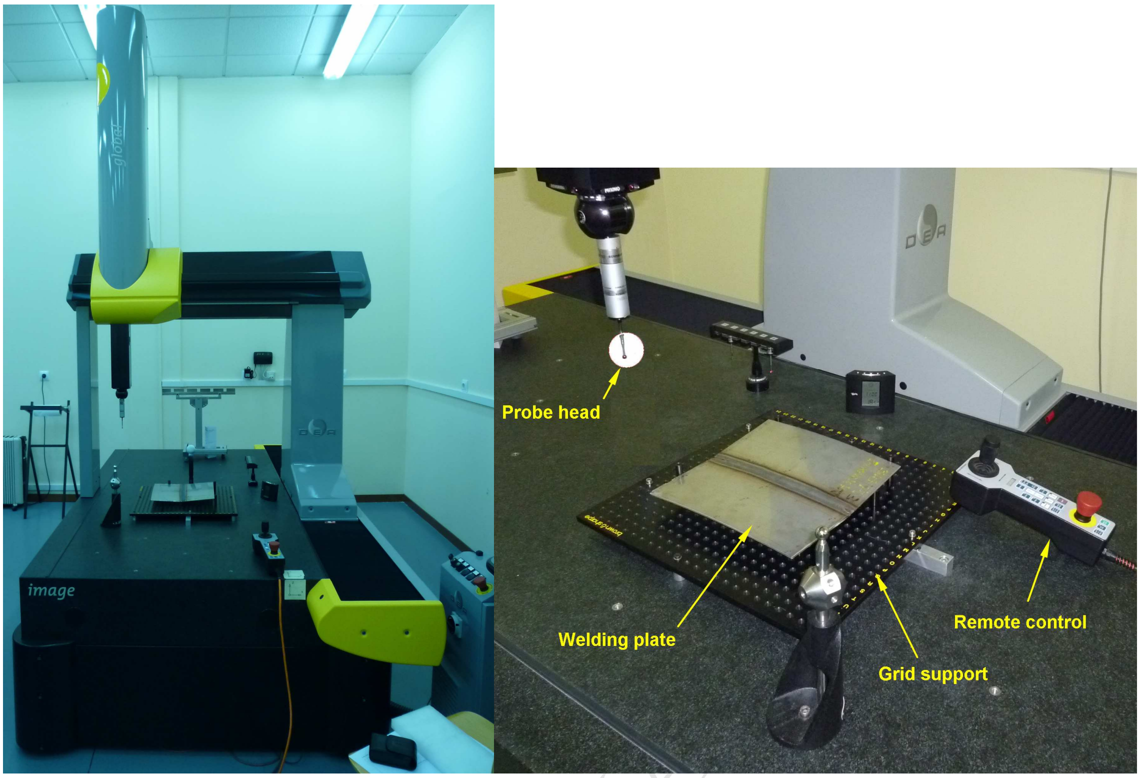

Fig. 9. Experimental setup of the coordinate measuring machine (CMM): overall view (left) and a detail (right).

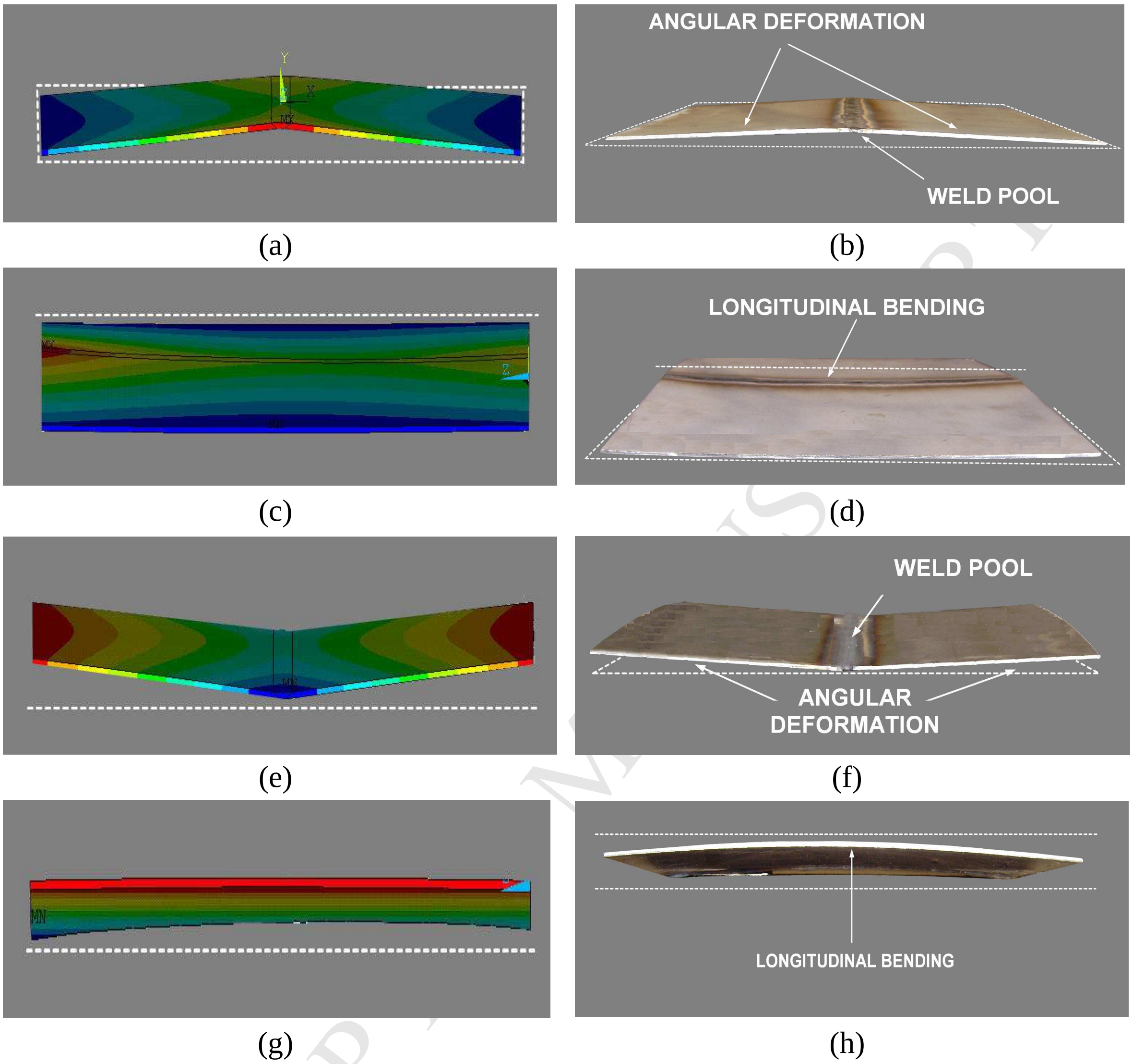

Fig. 10. Comparison between the experimental deformed shape (left, a, c, e, g) and the numerical results (right, b, d, f, h).

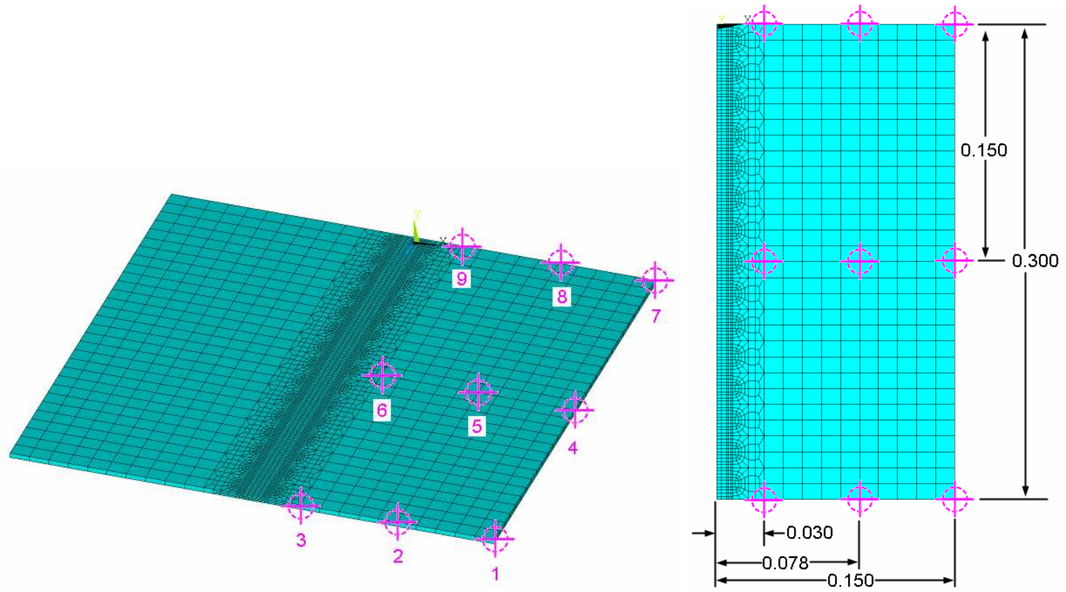

Fig. 11. Geometrical description of the locations considered for results comparison.

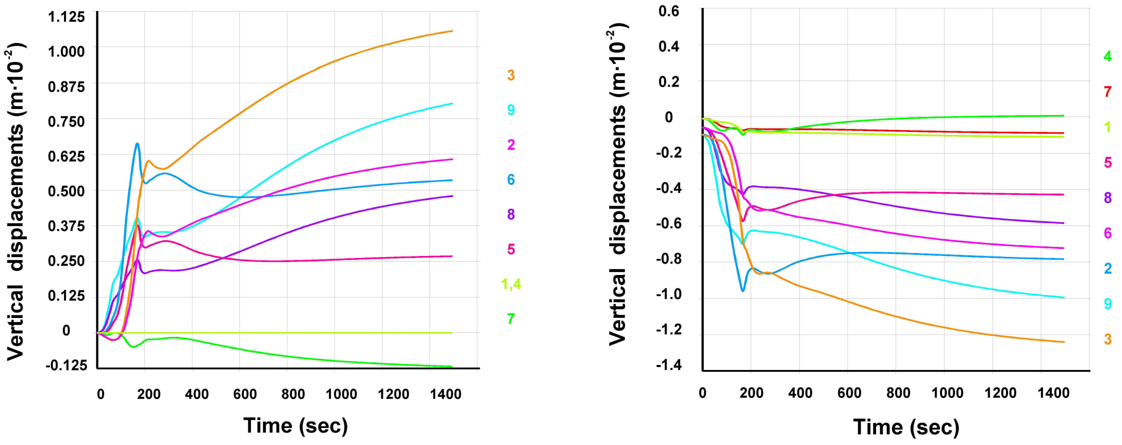

Fig. 12. Vertical displacement evolution at nine different locations for both specimens: duplex stainless steel plates (left) and austenitic stainless steel (right).

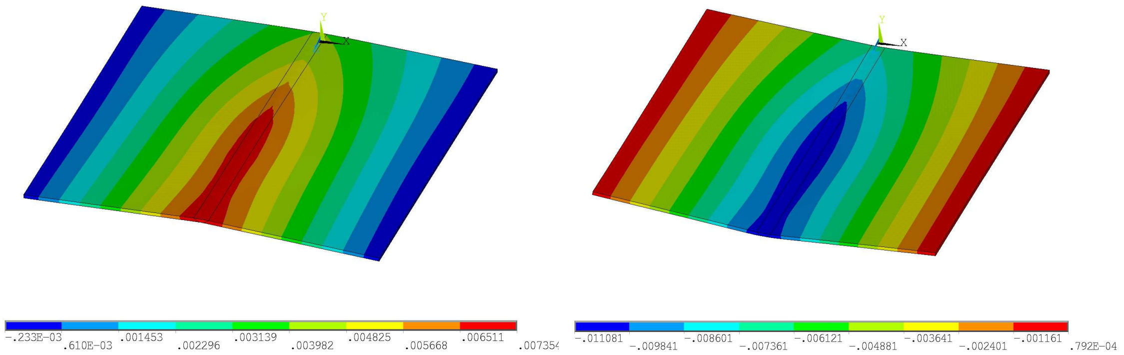

Time: 274 s

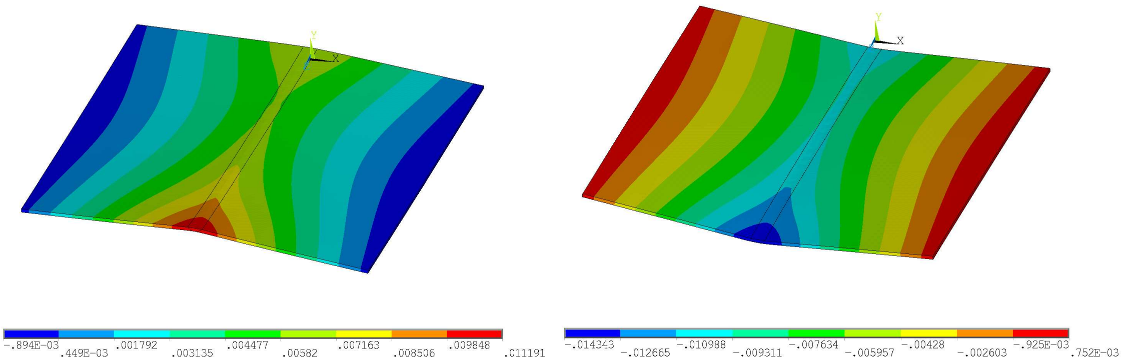

Time: 780 s

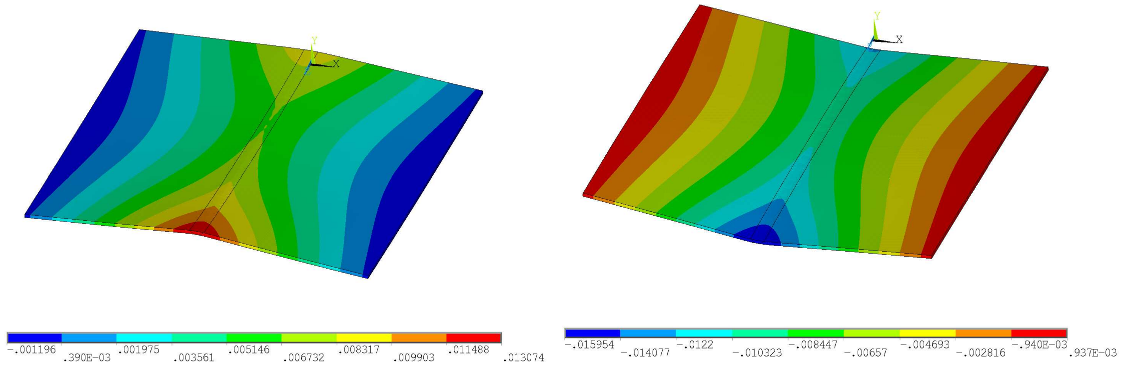

Time: 1,300 s

Fig. 13. Numerical FEM displacement results for duplex (left) and austenitic (right) stainless steels in three different time steps.

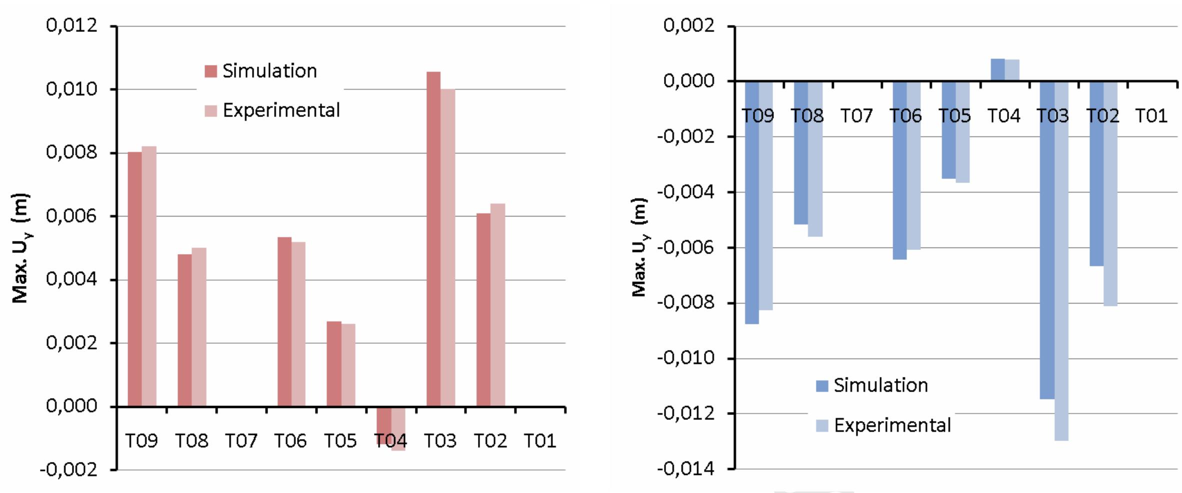

Fig. 14. Comparison between vertical displacement values at selected locations for duplex (left) and austenitic (right) stainless steel. Numerical simulation vs experimental results.